Design of a Thermal Testbed for Metrology of Active Antennas

Bryan L. Schoenholz, James M. Downey, Marie T. Piasecki
NASA Glenn Research Center
Cleveland, Ohio, United States of America
bryan.schoenholz-1@nasa.gov

***Abstract*— NASA mission requirements have driven an increased interest in active phased array antennas (APAA) for space-based user communication terminals. Recent advancements in 5G technology have driven down the cost of APAA development and manufacturing all while providing a technology solution that covers many existing Ka-Band satellite communication spectrum bands. While these developments have provided ample opportunities to leverage new chips and arrays for use in space, there is also a need to evaluate these antennas in a relevant environment. Active arrays, as designed for use in 5G, require thermal management to avoid damage to the device as well as to maintain performance. Measured performance under various thermal conditions is essential both for understanding overall APAA performance and ensuring operation is within required tolerances. To address these measurement needs, the SmallSat Ka-band Operations User Terminal (SKOUT) project at the NASA Glenn Research Center (GRC) developed a test environment that combines traditional antenna and communication system metrology with a conduction cooling/heating thermal control system to simulate the space thermal environment. This paper will address the metrology system design and performance specifications as well as test article setup and operation. Tests that are typically performed at ambient temperature can now be performed over the typical temperature range of a Low Earth Orbit (LEO) mission. These tests include error vector magnitude (EVM), gain to noise temperature (G/T), antenna patterns, and non-linear characterization. The paper will cover the configuration for each test and provide results from a recent test campaign. Results illustrate the importance of higher fidelity environmental testing when evaluating the performance of an APAA.**

I. Introduction

The National Aeronautics and Space Administration (NASA) has identified many applications in which the use of active phased array antenna (APAA) systems is advantageous [1]. These applications include both aeronautics and space environments and require operation over large temperature ranges. For example, a typical low earth orbit (LEO) payload can be subject to temperatures ranging from -65 C to +125 C [2]. Even with a thermal management system, a component operational temperature could be from -20 C to +60 C [3]. Since an APAA system implements a network of amplifiers for both transmit and receive the composite system is subject to non-trivial performance changes over these temperature ranges. To mitigate mission risk, it is necessary to characterize an APAA's performance over temperature before flight to allow proper communication system design.

Thermal testing of electronic components over a large temperature range is typical in space flight qualification. There have also been examples of antenna pattern characterization for passive antennas over large temperature ranges [4] as well as return loss measurements in thermal vacuum chambers [5]. The challenge of managing an active antenna's thermal load while conducting antenna radiation measurements however is less common. This testing requires a thermal test system which can be integrated into a flexible antenna test facility. The NASA Glenn Research Center (GRC) has developed a system to control the baseplate temperature of a microwave APAA from -40C to +60 C and integrated it with an existing Portable Laser Guided Robotic Metrology (PLGRM) system. The PLGRM is a robotic based antenna measurement system capable of various scan types [6]. With the combination of the thermal test system, the PLGRM and various microwave instruments, the following tests can be performed over a wide temperature range: effective isotropic radiated power (EIRP), radiation pattern measurements, gain over temperature (G/T), and nonlinear characterization including P1dB compression testing and error vector magnitude (EVM).

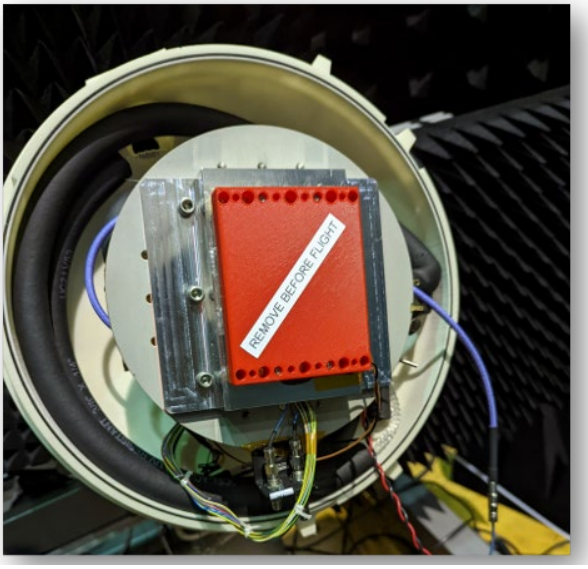

Figure 1. AUT on Thermal Plate without Dome

II. Thermal Test System Design

To simulate the thermal management system of a typical spacecraft the thermal test system itself was designed to be conduction based. The centerpiece of the design is a liquid cooled interface plate that is regulated with a thermo electric controller. The thermal plate can produce surface temperatures from -65 C to +200 C with the use of HT55 heat transfer fluid. This plate is then surrounded by a dome to control the ambient air around the APAA under test (AUT) and the cooling surface. The dome itself is constructed of a of a low dielectric constant (Dk) foam so that it remains transparent at microwave frequencies and has a negligible effect on the radiation of the AUT. Finally, a dry air purge is used to control the humidity in the enclosure which keeps ice from forming on the AUT at the low temperature points. The system is not pressurized by the dry air purge as there remains a leak point at the humidity sensor to ensure dry air continuously flows through the system and moisture can be carried out. The system then monitors and records temperatures on the thermal plate, AUT baseplate, inside enclosure air, and outside enclosure air as well as the humidity of the air inside the enclosure. Figure 1 above shows a conduction cooled AUT on the thermal plate. Figure 2 below shows a basic block diagram of the thermal system.

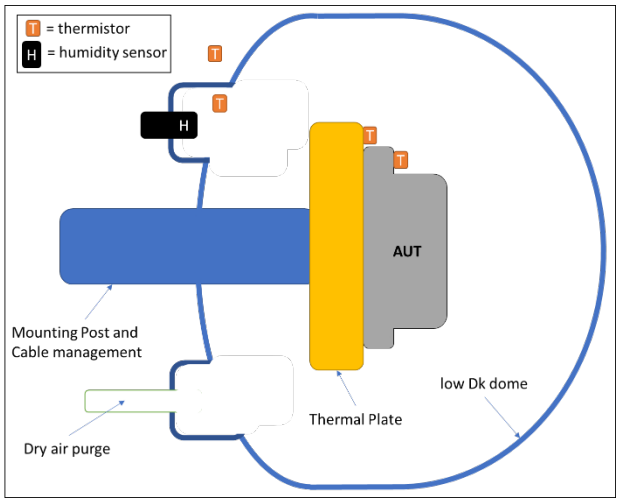

Figure 2. Thermal System Block Diagram

The Thermal Test system was characterized for RF performance by scanning a dual ridge horn both with and without the dome installed. Figure 3 shows the far field magnitude difference between the two scans. The dome contributes less than +/- 0.5 dB of magnitude or error on the AUT pattern for measurement angles within +/- 60 degrees.

III. RF Measurement System Design

The radio frequency (RF) measurement system is separated into two configurations: one for over-the-air (OTA) transmit testing and the other for radiation pattern and OTA receive testing. Figure 4 shows the OTA transmit test block diagram where an arbitrary waveform generator is used to source a modulated signal at an intermediate frequency (IF) which is then up converted to microwave frequencies. A coupler and power meter are used to measure the input power that is sourced to the

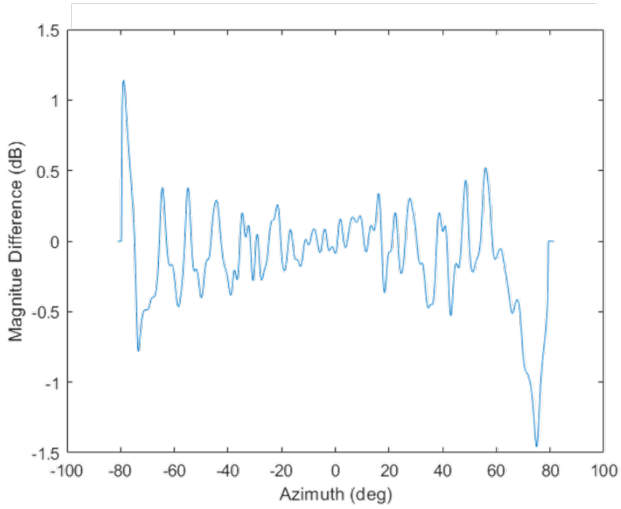

Figure 3. Magnitude Difference with and without Dome

AUT. The PLGRM's UR10 robotic arm is then used to position a linearly polarized open-ended waveguide (OEWG) probe to sample the beam in free space as pictured later in Figure 7. Finally, another coupler and power meter on the PLGRM are used to measure the AUT output power while a Signal Analyzer is used for spectral and vector measurements.

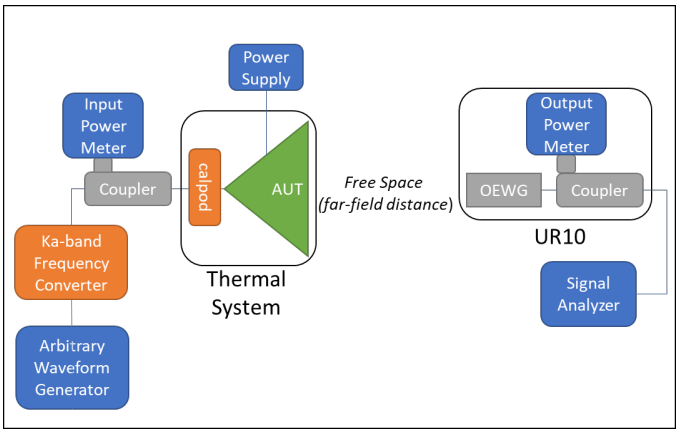

Figure 4. OTA Transmit Testing Block Diagram

The second configuration as shown in Figure 6 is used for radiation pattern characterization as well as OTA receive testing. In this configuration a vector network analyzer (VNA) is used to source and receive a continuous wave signal and when necessary added noise power. For radiation pattern measurements the PLGRM system can be used to sample the AUT's beam in both the near or far field as the probe spacing, scan type and scan extents are all flexible/programable.

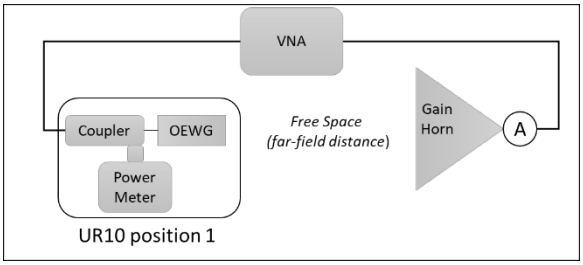

Figure 5. Range Loss Measurement Block Diagram

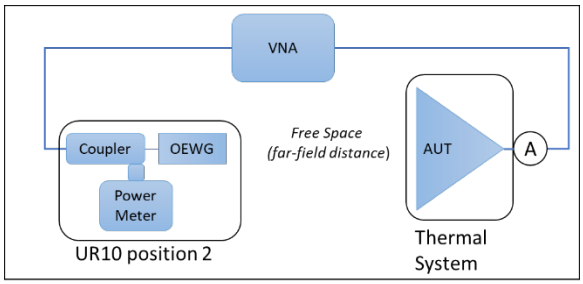

Figure 6. G/T and OTA Receiver Testing Block Diagram

G/T is the primary metric for OTA receiver testing. For G/T testing the system implements a cold source substitution method as outlined in [7]. In this test the AUT beam is sampled in the far field to ensure accurate gain measurement are made. Due to the nature of the substitution method the range loss is first measured using a standard gain horn. This requires the UR10 to move between 2 positions. Position 1 for the range loss measurement in Figure 5 and Position 2 for the AUT measurement in Figure 6. Port A in each diagram denotes the calibration plane and point at which the cable is moved from the reference measurement or to the AUT measurement. The PLGRM system enables convenient and accurate positioning of the OEWG to establish movement between the two positions using pre-programmed states. This enables quick system drift checks if necessary. The image in Figure 7 below shows the UR10 in Position 2 as it points to the AUT located inside the thermal test system.

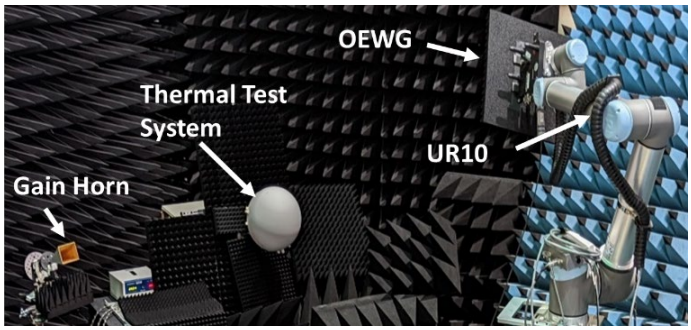

Figure 7. Integrated PLGRM and Thermal Test System

For all configurations thermal cycling of the RF cable within the dome subjects the measurements to amplitude and phase variations. This is particularly critical in G/T measurements and in near field radiation pattern scans. Amplitude error is directly proportional to gain error in the G/T measurement while phase error during near field sampling will change the near to far field transform as quantified in [8]. Errors in amplitude and phase were kept to a minimum by using an expanded polytetrafluoroethylene (ePTFE) RF cable [9] and short routing inside the dome. To ensure amplitude and phase changes were kept to a negligible level, a CalPod, or in-line temperature compensated VNA calibration standard, was installed at the connection point to the AUT and monitored over various temperature cycles. The variations were less than the correction range of the CalPod: +/- 0.1 dB in amplitude and +/- 1.5 degrees in phase at Ka-Band.

IV. Measurment Data

The AUT tested for this paper was a circularly polarized Ka-band APAA and produced as much as 80 watts of heat load. The AUT baseplate temperature range tested was -20 C to +40 C. The test signal used for OTA transmit testing in these measurements implemented offset quadrature phase shift keying (OQPSK) modulation at 333M samples per second on an IF of 5 GHz. The IF signal was up converted to 27.1 GHz and final input power levels to the AUT were set using a variable gain attenuator in the upconverter. In all tests the thermal test system was set to control the AUT baseplate temperature to a target steady state point before RF data collection was performed. Increasing the AUT EIRP increases heat load and decreasing operational temperature increases the system thermal losses which leads to changing settling times between the various points collected. As such, all RF data was automatically collected, and time stamped to eliminate user error and ensure transient temperature changes did not affect the results.

OTA transmit tests included EIRP, P1dB point testing, and EVM. All OTA transmit test links used an AUT to OEWG separation of 2.8 meters to ensure far field sampling for the tested APAA. The EIRP value is calculated using equation 1 below.

$$EIRP = P_{out} + FSPL + L_p - G_{oewg} \quad (1)$$

Where P_{out} is the raw output power meter reading, FSPL is the free space path loss of the link at 2.8 meters, L_p is the polarization loss between the linear OEWG and circularly polarized AUT (3 dB was used in this test case), and G_{oewg} is the gain of the OEWG. To increase accuracy of L_p orthogonal polarization measurements can be made to account for axial ratio mismatch.

Figure 8 shows compression test results for 4 operational temperatures: -20, 0, 20 and 40 C. As expected, the achievable EIRP of the AUT increases as the baseplate temperature is lowered. Notably, the shape of the compression curve changes with temperature. A linear fit is drawn to for each temperature point and P1dB points are marked as a baseline for further analysis.

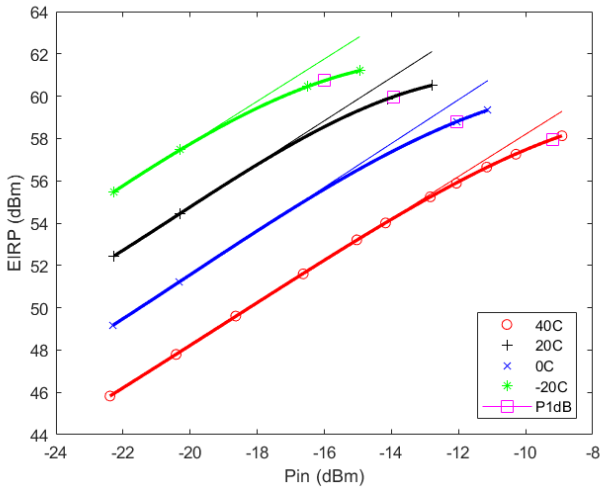

Figure 8. Pin vs Pout over Temperature

Figure 9 below shows the trend of EIRP and DC power consumption over temperature using the above calculated P1dB points. Again, as expected the EIRP and DC power consumption both increased as temperatures decreased.

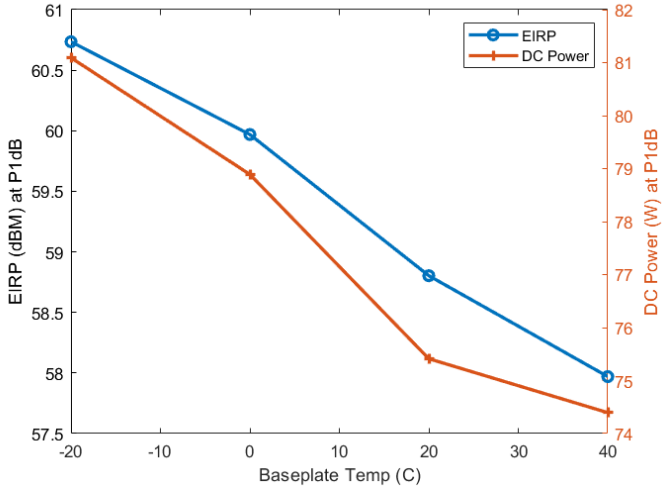

Figure 9. EIRP and DC Power consumption over Temperature

Figure 10 also uses the calculated P1dB points and plots both EVM and EIRP at P1dB over temperature. Though higher EIRP is achieved at lower temperatures the EVM performance suffers. This correlates to the changing derivative of the compression curve across temperature as observed in Figure 8 This information will be useful for system designers to determine the appropriate back off for the AUT to achieve a desired link performance. It is clear from this data that changes in performance over temperature will need to be accounted for in the communication system mission design.

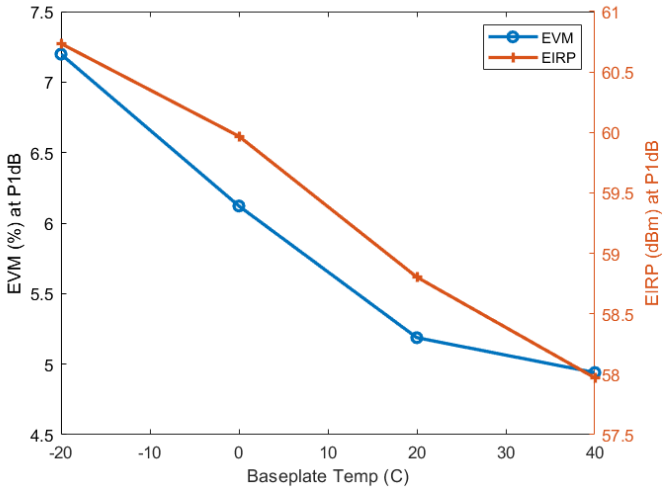

Figure 10. EVM and EIRP over Temperature

The final OTA test used to characterize the performance of the APAA is G/T. Since the OEWG is linearly polarized both horizontal and vertical polarization measurements were collected so that the measurements can be combined to calculate the gain for circular polarization accordingly. Equations 2 and 3 are used to calculate the final G/T for the various temperature points:

$$DUTNPDI = DUTRNPI + 10*\log_{10}(T) \quad (2)$$

$$G/T = S21_{APAA} + G_{STD} - S21_{RL} - DUTNPDI. \quad (3)$$

Where DUTNPDI is the maximum noise power provided by a device under test (DUT) into a matched load, DUTRNPI is the device under test relative incident noise power defined by the ratio of the DUT temperature to 290 Kelvin, T is the room temperature in Kelvin, $S21_{APAA}$ is AUT measurement S-parameters, G_{STD} is the gain of the standard gain horn used in the range loss measurement, and $S21_{RL}$ is the range loss S-parameters.

Figure 11 below shows the results for G/T over the AUT's operational frequencies at the 4 temperature points. As expected, the system performs best at lower operating temperatures when G/T is the highest. This data again is necessary to allow an accurate link design for this AUT since the G/T performance varies more than 4 dB over the tested temperature range.

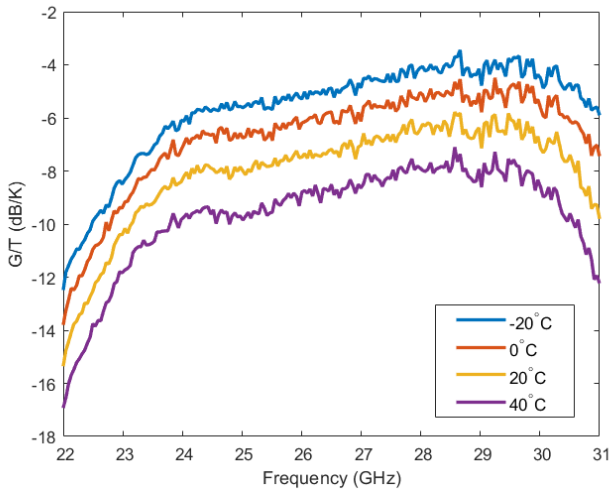

Figure 11. G/T over Temperature.

V. Conclusions

The design of a thermal test system was presented to vary the baseplate temperature of a Ka-band APAA over its expected operational temperatures. These temperatures simulate a typical LEO mission profile. The integration of this thermal test system with the previously presented PLGRM system enables real world antenna characterization and validation of antenna performance over its designed operational temperature range. The test results show changing compression behavior over the temperature range. Understanding these changes will be valuable for optimizing a mission communications link using the tested APAA.

Acknowledgement

The authors would like to acknowledge the Space Communications and Navigation (SCaN) program and the SmallSat Ka-band Operations User Terminal (SKOUT) project for supporting the development of the thermal test system as well as the APAA used as the antenna under test. The authors would also like to acknowledge the Transformative Aeronautics Concepts Program (TACP) for supporting the continual development of the PLGRM System.

References

[1] J. A. Nessel, J. M. Downey, B. L. Schoenholz, M. T. Piasecki and F. A. Miranda, "Potential Applications of Active Antenna Technologies for Emerging NASA Space Communications Scenarios," in *14th European Conference on Antennas and Propagation (EuCAP)*, 2020.

[2] J. Plante and L. Brandon, "Environmental Conditions for Space Flight Hardware: A Survey," NASA Technical Reports Server, Washington D.C., 2005.

[3] V. Baturkin, "Micro-satellites thermal control—concepts and components," *Acta Astronautica,* vol. 56, no. 1-2, pp. 161-170, 2005.

[4] L. J. Foged, A. Giacomini and R. Morbidini, "Thermal testing of antennas in spherical near field multi-probe system," in *5th European Conference on Antennas and Propagation (EUCAP)*, 2011.

[5] J. R. Dennison and M. G. Bray, "Radial Line Slot Array Antenna High Power Thermal Vacuum Testing," in *IEEE International Symposium on Antennas and Propagation and North American Radio Science Meeting*, 2020.

[6] P. A. Slater, J. M. Downey, M. T. Piasecki and B. L. Schoenholz, "Portable Laser Guided Robotic Metrology System," in *Antenna Measurement Techniques Association Symposium (AMTA)*, San Diego, 2019.

[7] J. Dunsmore, "OTA G/T Measurements of Active Phased Array Antenna Noise using a Vector Network Analyzer," in *94th ARFTG Microwave Measurement Symposium (ARFTG)*, 2020.

[8] W. Chen, C. Hu, S. Li, S. Guo, L. Gou and K. Zheng, "Influence of amplitude and phase errors on near-field to far-field transformation," in *IEEE International Symposium on Antennas and Propagation & USNC/URSI National Radio Science Meeting*, 2017.

[9] "Technical Information: Changes in Insertion Loss and Phase," Gore, [Online]. Available: https://www.gore.com/resources/technical-information-changes-insertion-loss-and-phase. [Accessed 30 July 2022].